

# Real-Time, Programmable, Digital Signal-Processing Electronics for Extracting the Information from a Detector Module for Multi-Modality PET/SPECT/CT Scanners

Dario B. Crosetto

900 Hideaway Pl, DeSoto, Texas 75115  
Crosetto@att.net, Dario.Crosetto@cern.ch

## *Abstract*

Measurements performed by manufacturers on their PET devices reveal a limitation of the electronics in extracting the properties of particles hitting the detector. As a consequence, either a lead collimator with holes is placed in front of the detector (2-D mode) preventing many photons which are not sufficiently aligned with the holes from ever reaching the detector, or many photons are lost because the electronics cannot fully process the data and separate the good event from the bad events. In order to overcome the above limitation, a data acquisition system based on the programmable 3D-Flow processor has been designed for acquiring data from modules for multi-modality PET/SPECT/CT. The modular electronics allows for digital data to be acquired from all sensors included in a given view angle of the detector. Each channel can sustain an input data rate of 20 MHz, 64-bit word; 40 MHz, 32-bit word; or 80 MHz, 16-bit word. The bits at each electronic channel correspond to spatial, timing, and energy information from photomultipliers, Avalanche Photodiodes (APD), photodiodes, or other sensors. The programmable circuit performs digital signal-processing operations on the incoming bit string such as: (a) variable digital integration time (or pile-up identification/correction) which allows for the maximum count rate capabilities while preserving spatial resolution; (b) depth of interaction which reduces the parallax error based on pulse shape discrimination (PSD), and/or pulse height discrimination (PHD); (c) improvement of the signal-to-noise ratio; (d) centroid calculation to improve spatial resolution or/and techniques of most likely position given the statistical nature of the signals; (e) correlation with neighboring signals; and (f) improving the timing resolution from the information received from the time-to-digital converter and pulse shape analysis.

## I. INTRODUCTION

When the increase in sensitivity of a system corresponds to an even greater percentage increase of the noise, there is no benefit to the user. The observation made by Dr. Alan Waxman, director of the nuclear medicine Cedars-Sinai Medical Center in Los Angeles, i.e. that it was bad news to discover that the new PET systems are so sensitive to minute accumulations of  $^{18}\text{F}$ -FDG that it has become harder to tell the difference between malignancy and inflammation, indicates that this type of increase in sensitivity offers no advantages.

Conversely, an increase in sensitivity (see reference [1]) that allows for more “good photons” to be captured can only improve the image quality, showing details more accurately, and helping the physician recognize subtle differences in normal anatomy.

This article (a) analyzes and identifies the limitation of the electronics of the current PET which impede the extraction of particle’s properties as well as to recognizing the good photons and (b) it compares the techniques used in current PET with the new proposed techniques to overcome these limitations.

## II. FRONT-END ELECTRONICS OF THE 3D-FLOW SYSTEM VS. CURRENT PETS FE ELECTRONICS

The particle’s properties of the photon incident into the detector can be extracted from (a) the shape of the signal generated by the transducer (photomultiplier, APD, or photodiode, etc.); (b) the correlation of each signal with its eight (or twenty-four) neighbors in all four direction; and (c) the signal timing information telling when the event occurred.

The approach used in the electronics of the current PET of adding to each signal three neighboring signals from only one direction, prevents the particle’s properties from being further and fully accurately extracted. The shape of the resulting sum of the four signals has lost the information of each individual signal and from that point on it will be impossible to decompose the sum of four signals into individual signals. Furthermore, in the current PET, the sum of those four signals are not correlated with their neighboring sum of four.

If the particle’ properties are not fully extracted, the photons of the “good” events cannot be recognized with respect to the “bad” events. Consequently, the numerous bad events (noise) that were not subtracted at the very front-end electronics and that could not be subtracted with filtering algorithms at the back-end (unless several good events are extracted along with them), will fail to provide a clear image that will help the physician in recognizing subtle differences in normal anatomies.

The left side of Figure 1a displays the Digital Signal Processing (DSP) of the 3D-Flow system with digital signal integration functionality as opposed to the analog signal processing implemented in the current PET systems in Figure 1b.



which is converted to digital and mapped into the 3D-Flow input word in bits 50-56.

The decay-time (e.g.,  $d_A$  in Figure 2) is the difference between the time detected by the CFD2 after integration of the signal from the PMT (this time is proportional to the decay time of the crystal) and the previously detected time-stamp. The TDC produces the second time-mark, which is subtracted from the time-stamp of CFD1 and mapped into the 3D-Flow input word in bits 48-49 by the FPGA (see also Section 13.4.4.2, and Figure 13-6 of [1]).

Similarly the information from the other three detector blocks are mapped into the remaining sections of the 3D-Flow input data word.

The data received by the front-end electronics during a given 50 ns sampling time period (e.g.,  $t_3$ ), are sent in a pipeline mode, e.g., two sampling periods later, in order to allow the analog and digital electronics to propagate and convert to digital the signals (e.g., at time  $t_5$ ) to the 3D-Flow

electronics (see bottom left of Figure 2).

Example 2 shows a 64-bit word carrying the information from one or more transducers (PMTs, APDs, and/or photodiodes), coupled to a detector block made of slow crystals. Slow crystals have a long decay time of about 230 ns, which can be shortened to 200 ns. (Alternatively, the 3D-Flow CPU clock could be stretched). The detector provides the raw information of the ADC counts of the signals received every 50 ns, the time-stamp of the last two hits detected, and the position/DOI through photodiode and/or light sharing information..

Since the sampling time is 50 ns and the crystal decay time is expected to be on the order of 230 ns (shortened to 200 ns using the technique described in [3]), a buffer memorizes the last three samples. Each time a new sample of the input signal is acquired, the last value is grouped to the previous three samples and sent to one 3D-Flow DSP. The buffering function is implemented in the FPGA (see Section 13.4.4.3, and Figure 13-7 of [1]).

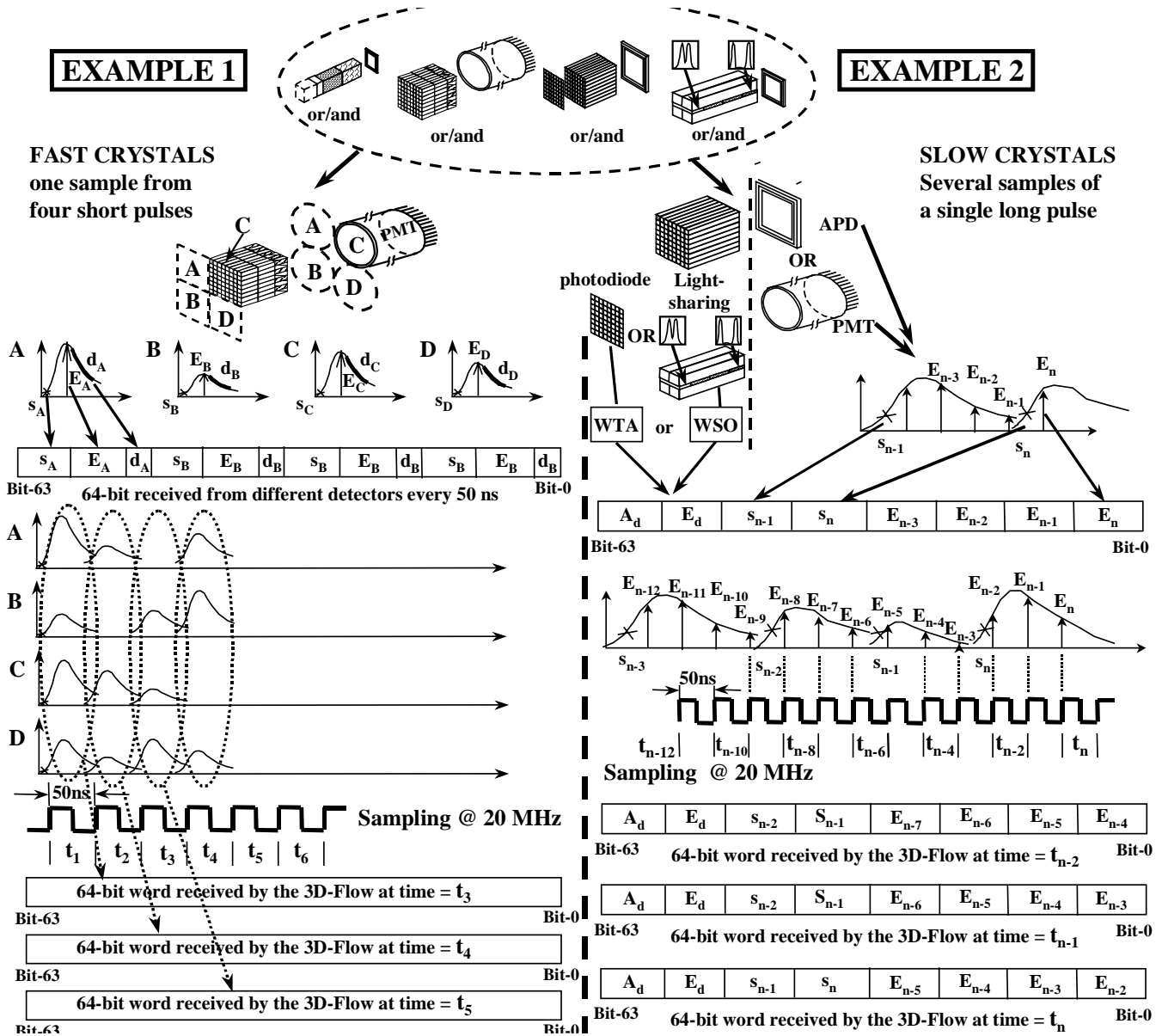


Figure 2. Examples of acquiring data by the 3D-Flow system, from the detector.

The bottom right of Figure 2 shows that the amplitude of the signals  $E_{n-3}$ ,  $E_{n-4}$ ,  $E_{n-5}$ , and  $E_{n-6}$ , are sent at time  $t_{n-1}$  to the 3D-Flow and that the amplitudes of the signals  $E_{n-2}$ ,  $E_{n-3}$ ,  $E_{n-4}$ , and  $E_{n-5}$ , are sent at time  $t_n$  to the 3D-Flow. The above four 8-bit values of signal amplitude information (ADC counts) are mapped to the 3D-Flow input word in bits 0-31. Data are sent to the 3D-Flow system in a pipeline mode, e.g. two sampling periods later than the receiving time from the detector. This allows the analog and digital electronics to propagate, convert to digital, and align the time of signals belonging to the same event. Signals belonging to the same event are produced at different times because the transducers have different response times. (See reference [4] for the conceptual design down to the circuit description in graphic form and in VHDL form of the interface that aligns signals between different detector/transducer types with different response times.)

The rising edges of the signal from the PMT (or APD) above a certain threshold are detected by the CFD1 with short delay (see Section 13.4.4.3 of [1]), and a logical signal is sent from the CFD1 output to the time-to-digital converter (see Section 13.4.10 of [1]). This, produces a 9-bit time-stamp (e.g.,  $s_n$  in Figure 2), which is mapped in the 3D-Flow input word in bits 32-40. More bits for the time-stamp are needed in example 2 with respect to example 1, because, while the 500 ps resolution of the TDC is the same, the duration of the decay is longer (from 40 ns to 200 ns), and the longer time measurements require more bits. The previously recorded time-stamp (e.g.,  $s_{n-1}$  in Figure 2) in the FPGA buffer is mapped in the 3D-Flow input word to bits 41-49.

Either technique -- ratio of signals from photodiode and PMT [5, 16] or the light sharing technique [18] -- can be used in the 3D-Flow system.

In the case of the use of a scintillator crystal coupled to the PMT at one end and at the other end to 64 photodiodes (PD), the following observations can be made:

- a) the crystal of interaction can be identified by the PD with highest signal;
- b) the sum (PD + PMT) contributes to calculate the total energy, and
- c) the ratio PD/(PD + PMT) determines the depth of interaction.

The 3D-Flow can perform the operations of addition and division to extract the photon's characteristics from the raw data that are provided by the "winner-take-all chips" (WTA) [15]. These are interfaced to the 64 PD and which produce one analog signal of the highest PD and its relative 6-bit address. The analog signal converted to 7-bit digital (e.g.,  $E_d$  in Figure 2) can be mapped into the 3D-Flow input word at bits 50-56 and its relative address (e.g.,  $A_d$  in Figure 2) at bits 57-62. Thus, one spare bit of the 64-bit 3D-Flow input data word remains.

In case the light-sharing technique is used, then the information can be mapped into the 3D-Flow input word at bit 50-56 for the maximum+partner and bits 57-63 for their address. This technique makes use of the "winner-select-output" (WSO) [17] chip, which provides the analog signal

with the highest amplitude called "maximum," and second highest signal called "partner."

#### IV. MEASUREMENTS ON CURRENT PET SHOWING AREA THAT NEED IMPROVEMENT

Figure 3 shows the limitation introduced by the presence of 2x2 PMT block boundaries of the current PET systems. The bottom section of the figure shows one of the several figures available in several publications [6, 7, 12, 8]. Although on Section II.C of [12] it is stated that "...Detector boundaries may form any appropriate shape to account for non linearities in the positioning response..." the much lower thresholds (see Figure 3 of [12]) used for the corner and edge crystals of the 2x2 block compared to the thresholds of the center crystals (which are also corner crystals of PMTs) indicates that the energy of the incident photons detected by the corner/edge crystals is much lower than that detected by the center crystals. This is because part of the energy of the incident photon is detected by the adjacent 2x2 block and is lost when using the approach of the current PET, because there is no communication between 2x2 PMT blocks. Instead, the center crystals (which are also corner crystals of the PMTs) have instead higher thresholds since the Anger logic [9] can account for the energy of the incident photon which was split among the four PMTs.

The proposed architecture of the 3D-Flow with no boundary between 2x2 PMTs provides a platform where all corner crystals will be like the ones currently located at the center of the 2x2 PMT block, or providing even higher accuracy by means of 3x3, or 5x5 neighbor clustering. Thus all measurements will be like the four crystals in the center of the 2x2 PMT block; no such difference of lower thresholds as the ones used in the current PET will be required, and the complete energy of the corner/edge crystals could be rebuilt as it is for the center crystals.

The current PET's arrangement of blocks with 2x2 boundaries (the 2x2 boundary is provided by the grouping of the 2x2 PMTs) causes different signals in different positions of the 64-, 144-, or 256-crystal block change the geometrical segmentation of the crystals into the layout of the crystal region boundary lines similar to the one shown in the bottom right of Figure 3 (see the crystal-region boundary lines in Figure 3 of reference [7]). The signal at the corner of the 2x2 PMT block (see Figure 3b1) has a high component of noise and only a fraction of the signal (about 50 ADC counts. See measurements performed in [6] on the left of Figure 3) of the incident photon. The other part of the signal is in the adjacent 2x2 PMT block and is lost because there is no communication among the two blocks. Figure 3b2 shows a much higher signal (about 150 ADC counts) corresponding to the crystal directly over the PMT photocathode (see measurements performed in [16] on the right of Figure 3). Figure 3b3 shows the estimated signal (as described from measurements in several articles) at the center of the 2x2 PMT block, which corresponds to a corner crystal in between 4 PMTs.

# Current PET systems

- **Boundary limitation at the block and module segmentation.**
- **Missing the detection of photons at the block boundaries, poor S/N ratio and lack of Signal Processing**
- **Fixed, hard-wired architecture for 2x2 centroid**
- **Analog signal processing**

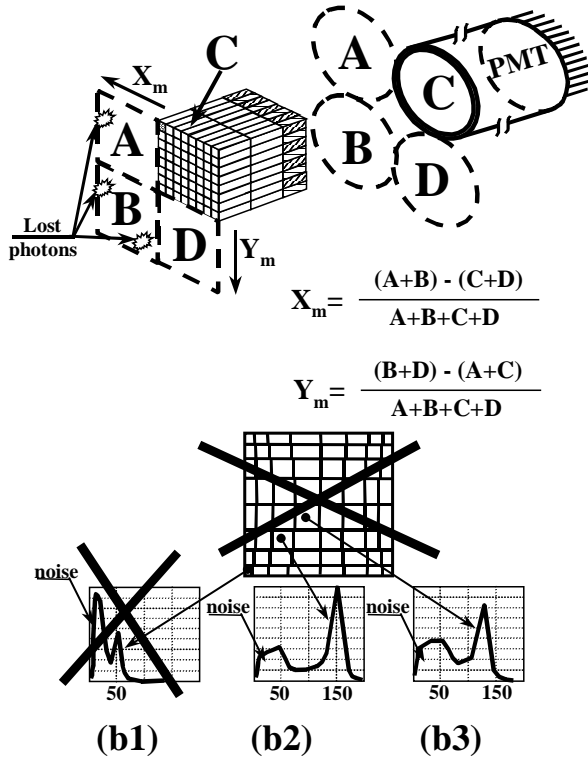


Figure 3. Measurements performed by manufacturers on current PET are reported in several articles. The measurements show an unequal signal response when a photons hits different areas of the detector. When a photon hits the detector in a corner (see section 1b of the figure) of a 2x2 block or at the edge of the block, the photon is lost because its energy is split between two 2x2 modules which do not exchange information.

## V. DIGITAL SIGNAL PROCESSING ON EACH CHANNEL

The efficiency in identifying photon candidates for coincidence detection in the PET and identifying the source type (60 keV, from x-ray, 140 keV from SPECT, and 511 keV from PET) can be improved by using DSP techniques on signals received from each channel of the detector. The 3D-Flow system [10] allows for implementation of real-time digital signal processing on each channel and correlation with neighboring channels in real-time with zero dead time and with the capability of executing an algorithm whose execution time is longer than the time interval between two consecutive input data.

The parallel processing approach of the 3D-Flow compares with the current approach [11, 12] based on fixed 2x2 blocks as shown in Table 1.

The entire 3D-Flow system is synchronous with a proposed sampling time of 50 ns (the sampling time can be changed to best match the decay time of the crystal used).

In the PET implemented with the 3D-Flow system [13], the geometry of the PET sensors are mapped to a 3D-Flow processor array in a manner that allows the exchange of information among the adjacent PET sensors through short signal delay.

Table 1. Comparison of a parallel DSP system with the 2x2 block system of the current PET

3D-Flow system	Current PET systems
<ul style="list-style-type: none"> <li>- NO boundary limitation, NO duplication of events</li> <li>- Suitable for “continuous”[14] or “block” detectors</li> <li>- Flexible clustering/centroid 2x2, 3x3, 4x4, or 5x5, etc.</li> <li>- The energy of each PMT is checked if it is the head of a cluster against its neighbors (3, 8, 15, or 24), easy identification of 60 keV, 140 keV, 511 keV by summing energy of neighboring detector elements.</li> <li>- Digital integration allowing for implementation of several depth-of-interaction techniques based on pulse shape discrimination (PSD) and/or pulse height discrimination (PHD) (or techniques such as: crystals with different decay times, Miyaoka/Lewellen with light sharing and ratio information, or Moses/Derenzo signal ratio from sensors coupled at both ends of a crystal).</li> </ul>	<ul style="list-style-type: none"> <li>- Boundary limitation at the block and module segmentation</li> <li>- Poor S/N ratio and lack of signal processing</li> <li>- Fix hard-wired architecture for 2x2 centroid</li> </ul>
Digital Signal Processing, high S/N ratio.	

The entire 3D-Flow system is a single array with no boundary limitation. The neighboring of sensors in the PET detector array is reflected with an identical neighboring scheme in the 3D-Flow processor array. Each channel (defined as all signals, from all subdetectors within a given view angle) in the 3D-Flow processor array, sends its information to, and receives their information from, its neighbors. This is equivalent to the exchange of information among adjacent channels (or sensors) in the PET detector array. The practical implementation of the data exchange between neighbors is shown in detail in Figure 15-7 of [1].

Once all data from each channel and its neighbors are moved into a single processing element, any pattern recognition-algorithm, and/or signal-to-noise filtering algorithm well known in the literature can be applied by using the DSP functions of the 3D-Flow processor. This is achieved with the instructions of arithmetic and logic operation including multiply-accumulate and divide.

These operations are accomplished in parallel on each channel. In the example of the application of Section 17 of [1], for instance, each of the 2,304 processors of one layer of the 3D-Flow stack executes in parallel the real-time algorithm, from beginning to end, on data received from the PET detector, while processors at different layers of the 3D-Flow stack operate from beginning to end on different sets of data—or events—received from the PET detector..

The centroid calculation with the 3D-Flow is straightforward after having gathered the information of 3, 8, 15, or 24 neighbors in a single processor, as is described in

Section 13.4.1.2 for a 3x3 centroid calculation and in Section 13.4.11.3 of [1] for a 5x5 centroid calculation.

One example of a more accurate centroid calculation compared to the 2x2 example show on Figure 3 is for the calculation of  $\Delta_x$  the ratio of the sum of the energies of all sensors at the west of the central element, divided by the sum of all sensors at the east of the central element ( $\Delta_x = \Sigma E_W / \Sigma E_E$ ). Similarly for the calculation of  $\Delta_y$  the ratio of the sum of the energies of all sensors at the north of the central element, divided by the sum of all sensors at the south of the central element ( $\Delta_y = \Sigma E_N / \Sigma E_S$ ). Accuracy and algorithm execution speed will determine whether a ratio or a subtraction is needed (the subtraction algorithm is a faster hardware operation).

The complete energy of the incident photon can be rebuilt

by adding to the channel with the highest energy (head of a cluster), the energy values of the 3x3, or 4x4 surrounding the channels. Alternatively, when larger areas of 5x5 or 6x6 are added, the complete energy of photons which went through crystal scatter can be rebuilt.

Increasing energy accuracy will improve spatial resolution, scatter rejection/acceptance, and attenuation correction.

Figure 4 shows an example of the execution on the 3D-Flow processor of a real-time algorithm which extracts the properties of the incident photon.

In the synchronous 3D-Flow system, every 50 ns, upon reception of the 64-bit word from the FPGA, all processors of one layer of the 3D-Flow stack execute the following steps in parallel (see Figure 4):

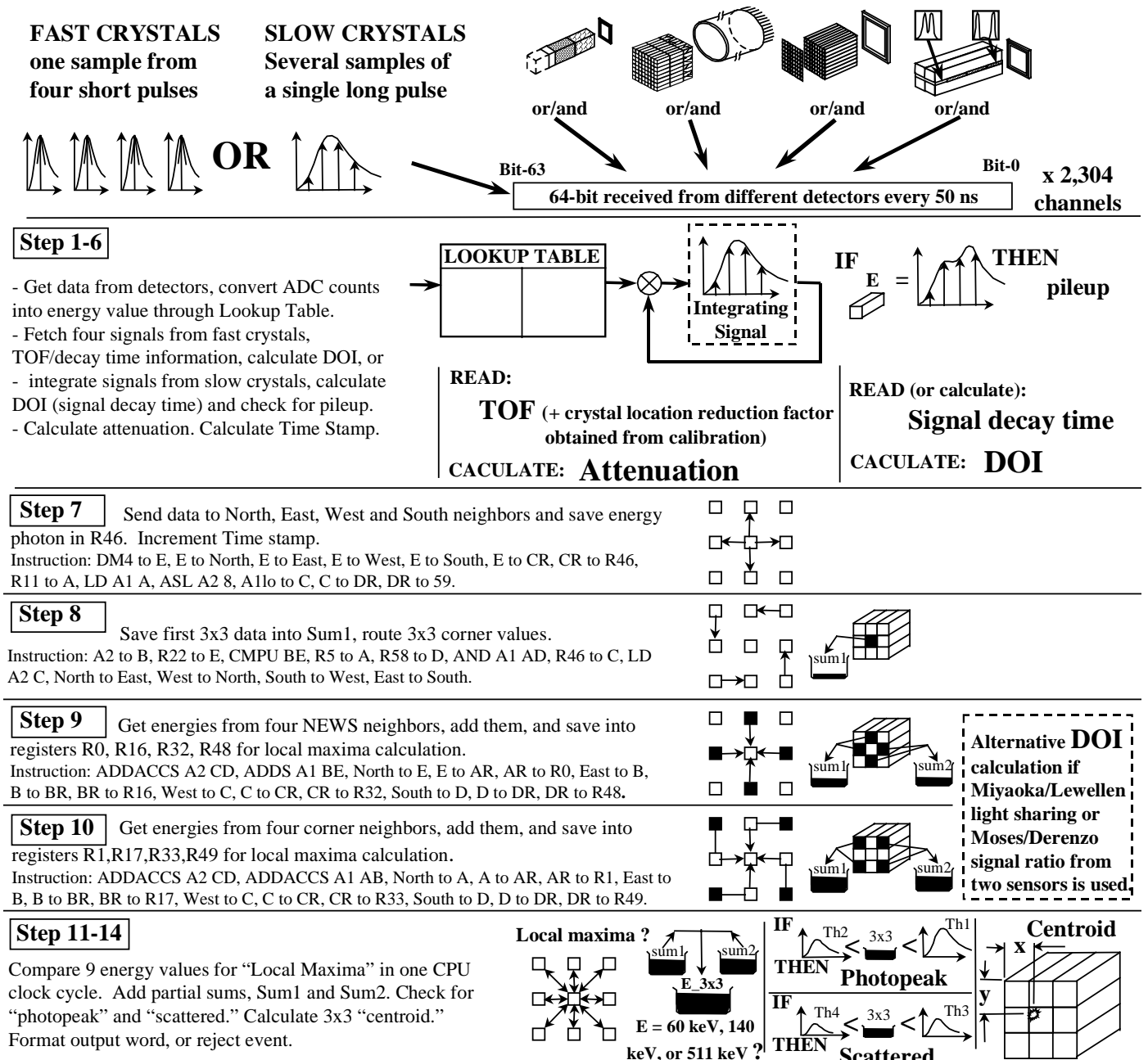


Figure 4. Simulation of the photon detection algorithm with the 3D-Flow for PET/SPECT/CT.

- Get data from detectors, convert ADC counts into energy value through Lookup Table.
- Fetch four signals from fast crystals, TOF/decay time information, calculate DOI, or integrate signals from slow crystals, calculate DOI (signal decay time) and check for pileup.
- Calculate attenuation; calculate Time Stamp.
- Send data to North, East, West and South neighbors and save energy photon in R46. Increment Time stamp.
- Save first 3x3 data into Sum1, route 3x3 corner values.
- Get energies from four NEWS neighbors, add them, and save into registers R0, R16, R32, R48 for local maxima calculation.
- Get energies from four corner neighbors, add them, and save into registers R1, R17, R33, R49 for local maxima calculation.
- Compare 9 energy values for “Local Maxima” tests whether the energy of the central cell is larger than any of its neighbors. (This operation is executed in one CPU cycle). Compute the total energy sum of 3x3 array by adding the partial sums, Sum1 and Sum2. Check for “photopeak” and “scattered.” Calculate 3x3 “centroid” compute the energy asymmetries, for subsequent determination of the point of impact ( $\Delta_x = E_W - E_E$  and  $\Delta_y = E_N - E_S$ .) Format output word, or reject event.

At this stage of the real-time algorithm there is much information computed that allows conclusions to be drawn, whether the photon is a 60 keV (x-ray), 140 keV (SPECT), or 511 keV (PET), and if attenuation, DOI, timing, spatial information are available. Any further operation can be executed upon 9 data (the one received from the detector and its 8 neighbors) by the CPU of the 3D-Flow processor, which can, in a single cycle, execute up to 26 operations of a standard computer.

## VI. DOI MEASUREMENTS FOR THE ELIMINATION OF THE PARALLAX ERROR

An oblique penetration of an incident photon into a crystal generates a parallax error if the depth of interaction (DOI) is not measured.

During the past 14 years, different techniques have been used to measure the DOI. The digital signal processing capabilities of the 3D-Flow system offer the possibility of implementing several of these. Figure 5 shows the block diagram of the logic to implement some of them.

Several techniques can be used, e.g. the signal ratio from sensors which uses a set of information including address bits from a WTA chip [15] and the analog amplitude pulse converted to digital for DOI technique with photodiode [16] or the address bits from a WSO [17] chip and the analog amplitude pulse converted to digital for DOI technique with light sharing [18].

## VII. DETECTION AND SEPARATION OF PHOTONS AT DIFFERENT ENERGIES

Detector modules have been tested for detecting photons at different energies (see top of Figure 5), by Saoudi and Lecomte [19] combining three crystals (GSO/LSO/CsI(Tl) in a phoswich to detect the photons at 60 keV, 140 keV, and 511 keV. The electronics with the 3D-Flow can recognize the three energies by means of digital signal processing and neighboring signal correlation. (See also Section 11.2.2.8.3 of [1]).

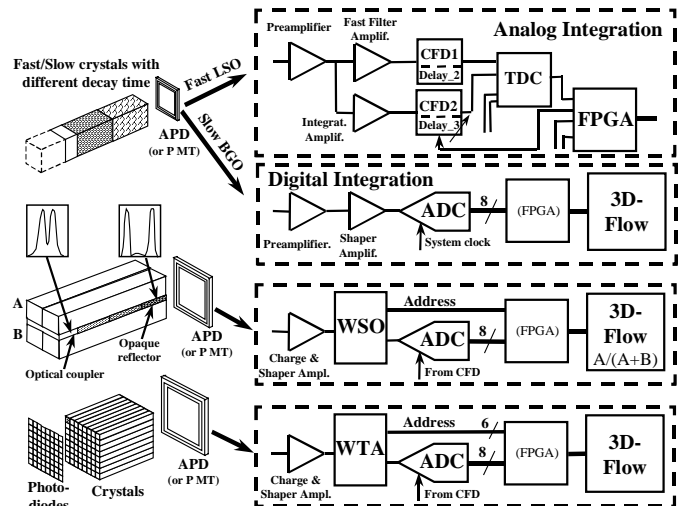


Figure 5. Flexibility of the 3D-Flow architecture in using different techniques to measure DOI.

## VIII. CONCLUSIONS

The article shows the area of limitation of the electronics of the current PET and sets forth the remedy for improvements.

The 3D-Flow architecture with a DSP on each channel allows for particle’s properties of the photon incident into the detector to be extracted from: (a) the shape of the signal generated by the transducer (photomultiplier, Avalanche Photodiode (APD), or photodiode, etc.); (b) the correlation of each signal with its eight (or twenty-four) neighbors in all four direction; and (c) from the signal timing information telling when the event occurred.

A good extraction of the particle’s properties results an ability to recognize the photons of the “good” events at the very front-end electronics and to reject the “bad” events. Consequently, more photons will be captured, requiring less radiation to the patient, allowing for faster scanning which reduces examination costs, and providing better image quality which helps the physician recognize subtle differences from normal anatomy, thus reducing “false positives.”

## IX. REFERENCES

[1] Crosetto, D. “400+ times improved PET efficiency for lower-dose radiation, lower-cost cancer screening.” ISBN 0-9702897-0-7. Available at Amazon.com.

- 
- [2] Binkley, D.M., et al.: A Custom CMOS Integrated Circuit for PET Tomograph Front-End Applications. IEEE, conf. rec. pp. 867 871, 1993.
- [3] Karp, J.S., et al.: Event localization in a continuous scintillation detector using digital processing. IEEE Trans. Nucl. Sci., vol. 33(1):550-555, February 1986.
- [4] Crosetto, D.: Detailed design of the digital electronics interfacing detectors... LHCb 99-006, 5 May, 1999 CERN – Geneva.
- [5] Moses, W.W., et al.: Performance of a PET detector module utilizing an array of silicon photodiodes to identify the crystal of interaction, IEEE, Trans. Nucl. Sci., vol. 40(4):1036-1040, August 1993.
- [6] Cherry, S.R., et al.: A comparison of PET detector modules employing rectangular and round photomultiplier tubes. IEEE Trans. Nucl. Sci., vol. 42(4):1064-1068 (Aug. 1995).
- [7] Rogers, J.G., et al.: Testing 144- and 256-crystal BGO block detectors. IEEE. Conf. Rec. Nuclear Sci. Symp. and Med. Imag., vol. 3, pp. 1837-1841, 1993.
- [8] Ficke, D.C., et al.: A GSO(Ce) block type detector for high count rate PET application. IEEE, conf. rec. 1994, pp. 1859-1863.
- [9] Anger R.T.: The Anger scintillation camera, Rao D.V., Ed.: Physics of Nuclear Medicine, Recent Advances, New York, American Institute of Physics, 1984.
- [10] Crosetto, D.: LHCb base-line level-0 trigger 3D-Flow implementation. Nucl. Instr. Methods A 436 (1999) 341-385.
- [11] Binkley, D.M., et al.: A Custom CMOS Integrated Circuit for PET Tomograph Front-End Applications. IEEE, conf. rec. pp. 867 871, 1993.
- [12] Cutler, P.D., et al.: Use of digital front-end electronics for optimization of a modular PET detector. IEEE Trans. Nucl. Sci., vol. 13, pp. 408-418, 1994.
- [13] Crosetto, D.: A modular VME or IBM PC based data acquisition system for multi-modality PET/CT scanners of different sizes and detector types. Presented at the IEEE Nuclear Science Symposium and Medical Imaging Conference, Lyon, France, 2000, IEEE-2000-563, submitted to IEEE, Trans. Nucl. Science.
- [14] Karp, J.S., et al.: Three-Dimensional Imaging Characteristics of the HEAD PENN-PET Scanner. JNM, vol. 38(4):636-643, April 1997.
- [15] Moses, W.W., et al.: A “winner-take-all” IC for determining the crystal of interaction in PET detectors. IEEE TNS, NS-43, pp. 1615-1718, 1996.
- [16] Huber, M.H., et al.: Characterization of a 64 channel PET detector using photodiodes for crystal identification. IEEE. TNS, vol 44(3):1197-1201, 1997.
- [17] Yu, H., et al.: A high-speed and high-precision Winner-Select-Output (WSO) ASIC. IEEE, conf. rec. Nucl. Sci. Symp. and Med. Imag., pp. 656-660, 1997.
- [18] Miyaoka, R.S., et al.: Design of a Depth of Interaction (DOI) PET Detector Module. IEEE Trans. Nucl. Sci., vol. 45(3):1069-1073, June 1998.
- [19] Saoudi, A., and Lecomte, R.: A Novel APD-based detector module for multi-modality PET/SPECT/CT scanners. IEEE Conf. Rec. Nucl. Sci. Symp. and Med. Imag., pp. 1089-1093, 1998.